RSC Advances

ROYAL SOCIETY OF CHEMISTRY

www.rsc.org/advances

Journal Name

Dynamic Article Links ▶

ARTICLE TYPE

Preparation of tungsten carbide nanosheets with high surface area by an in-situ DWCNTs template

Zi Ping Wu, *[a] Man Zhao, [a] Jing Wei Hu, [a] Wei Bo Zhang, [a] Yan Hong Yin,[a] Ying Yan Hu,[a] Ye Sheng Li, [a] Jian Gao Yang, [a] Qian Feng Xu [b] and Ajay Krishamurthy [c]

Tungsten carbide (WC) nanosheets were prepared using an in situ double-walled carbon nanotube (DWCNT) template with high dispersion. The growth of tungstenic acid (H_2WO_4) was restrained because of homogenous DWCNTs that were dispersed in ethylene glycol (EG). H_2WO_4 sheets about 50 nm long and 20 nm wide were obtained. WC nanosheets with high surface areas were prepared
10 when the tungstenic precursor was carbonized at a low temperature using a liquid carbon source. As the WC was used as precursor for depositing Pt nanoparticles, the obtained WC–Pt displayed a high electrochemical activity (Pt, 10 wt%). The results indicated that WC with a peculiar morphology and size could be used in electrochemistry, horniness alloys and other related fields.

1. Introduction

Tungsten carbide (WC) is an interstitial compound of C atoms
15 that are filled into a W crystal, which possesses high strength and rigidity as a covalent compound, high melting point as ionic crystal, and electromagnetism as a transition tool and surface coating [1–3]. However, horniness alloys are hardly formed through sintering because of the high melting point of WC. Once
20 the carbide size is reduced to the order of nanometers, the compaction temperature will be low and the sintering time will be reduced. Nano- and microsize WC can be compacted at 500 and 1200 °C, respectively [4]. In addition, nanosized WC exhibits a markedly improved strength, hardness, and tough sintered alloy
25 [5–8].

WC is gaining attention because of its high melting point and noble metal-like activity for commercial application to fuel cells [9–15]. Since 1960, WC has been used as anodic materials for hydrogen [16] or methanol fuel cells [17]. Studies have focused
30 on WC in chemical and electrochemical catalysis. The carbide is found to exhibit high stability in acidic solutions [18–20], and high toleration to carbon monoxide and bisulfide [21–23]. However, WC based anodic catalysts yield poor electrocatalytic activities, despite its resistance carbide to carbon monoxide
35 poisoning [24, 25]. The traditional metallurgical procedure is usually performed at high temperatures and yields materials with large particle sizes and low specific surface areas.

Nanosize WC can be used in a wide range of applications. Several methods have been proposed to synthesize the carbide,
40 such as the conventional furnace method based on direct interactions between elements, carbon-induced reduction of tungsten oxide [26], reduction of carbothermal hydrogen [27], and the reaction of tungsten with methane–hydrogen mixture [28]. However, the tradition methods exhibit difficulties during
45 preparation of nanosize WC with high specific surface areas because of high temperature, large size precursor, and insufficient interaction between tungsten precursor and carbon sources. In

addition, the morphology of the prepared WC is nanosized particles. However, to the best of our knowledge, few studies
50 focusing on WC with morphology of nanosheet have been reported [29, 30]. In this study, highly dispersive double-walled carbon nanotubes (DWCNTs) were used as carrier and template using an in situ approach to prepare well dispersed, small size WC precursors and deoxidize the oxides at low temperatures by a
55 liquid carbon source. For sufficient interactions between tungsten precursor and carbon sources, WC nanosheets with high surface areas could be prepared by the template. As the WC was used as precursor for depositing Pt nanoparticles, the obtained WC–Pt displayed a high electrochemical activity (Pt, 10 wt%).

60 ## 2. Experimental

2.1 Preparation of tungstenic acid (H_2WO_4)

H_2WO_4 was deposited on DWCNT bundles by direct precipitation with DWCNTs as in situ template. A homogenous DWCNT/ethylene glycol (EG) suspension was nondestructively
65 prepared as previously reported [28, 31–33]. The diameters of dispersed DWCNTs and DWCNT bundles were ~6 nm and 10–200 nm, respectively, the length of the nanotubes ranged from 1 μm to 2 μm. Following the preparation of the DWCNT/EG suspension, sodium tungstate (Na_2WO_4) was added into the
70 suspension. The complex suspension was transferred into a round flask for the tungstenic precursor. HCl was added into the suspension when the complex suspension was heated to 100 °C in a reflux device. The reaction temperature was sustained for 2 h, to enable sufficient H_2WO_4 deposition onto DWCNT bundles. The
75 as-received sample was cooled to room temperature, filtered, and washed with excess deionized water. The sample was then dried at room temperature in a low-vacuum system.

2.2 Carbonization of tungstenic precursor

The as-prepared precursor was carbonized by ethanol with a
80 single-step method. The prepared precursor was placed into a reaction furnace, and two flanges were applied on both ends of

RSC Advances Accepted Manuscript

reaction tube to seal the reaction chamber. The reaction system was drawn into a vacuum state prior to heating. After the reaction system was heated to 600 °C, air was pumped into tube at a flow rate of 300 ml min^{-1} for 1 h. High-purity nitrogen was then introduced into chamber at a flow rate of 300 ml min^{-1} and functioned as a protective gas. When the air was completely eliminated from the reaction chamber, the system was further heated to 950 °C. Ethanol was supplied into the reactor by an electronic squirming pump and nitrogen flow with a supply rate at 3 ml h^{-1}. The furnace was turned off and cooled to room temperature after 3 h. The received products were then collected from the furnace.

2.3 Pt deposition on tungsten carbide

Pt particles were deposited on WC in EG with a good dispersion state. EG was functioned as reduction and dispersion media. Accurately measured chloroplatinic acid (H_2PtCl_6) was added in the EG solution and then heated to 140 °C in a reflux device for 5 h. After cooling to room temperature, the as-received sample was filtered, washed with excess deionized water, and dried at room temperature in a low-vacuum system. Pt loading was controlled at 10 wt%.

2.4 Characterization of sample

The microstructure of sample was studied by high-resolution transmission electron microscopy (HRTEM, JEOL 2100F, accelerating voltage, 200 kV), Scanning electron microscopy (SEM, XL30), X-ray diffraction (XRD, D8 Advance, Bruker) by Cu Kα radiation, and thermogravimetric analysis (TGA, Diamond TG/DTA6300, heating rate, 10 °C min^{-1} from room temperature to 1000 °C at N_2 flow rate of 100 ml min^{-1}). Energy dispersive X-ray spectroscopy (EDS) was used to analyze the chemical composition of the selected area. N_2 adsorption and desorption isotherms of tungsten materials were measured at 77 K using a BELSORP instrument (BEL, Japan, Inc.), details about the analytical methods can be found in Ref. [34].

2.5 Electrochemical measurements

Electrochemical activities of WC–Pt materials were characterized by cyclic voltammetry (CV). Experiments were performed in a three-electrode cell using an EG & G potentiostat (CHI 618C) at room temperature. Working electrodes were prepared by spreading a catalyst coating and 5% Nafion mixture in ethanol on a glass carbon cylinder with a diameter of 3 mm. Pt loading of the working electrode was controlled at 0.2 mg cm^{-2}. A Pt foil and saturated calomel electrode (SCE) were used as counter electrode and electrolyte, respectively. CV profiles were recorded at a scan rate of 100 mV s^{-1} for potentials against SCE that ranged from −0.241 V to 0.999 V.

3. Results and discussion

Microstructures of semifinished sample that were prepared from DWCNTs/EG suspension, Na_2WO_4, and HCl were examined by SEM, HRTEM, XRD and TGA (Fig. 1). From Fig. 1a, it can observe that the sample has undergone self-assembly to form floccules. Several small particles deposition on the nanotube bundles is evident at higher magnifications of the floccules (Fig. 1b). Fig. S1a of the electronic supplementary Information (ESI) depicts the macro-morphologic feature of the material. It presents powder on macro-morphology. The sample was characterized using XRD further, characteristic peaks (Fig. 2a) with 2θ at 13°, 23°, 28.4°, 33.8°, 35.2°, 36.5°, 50°, 55.6° and 63.5° are observed,

which are indexed as planes of (010), (200), (011), (-201), (220), (221), (410), (420), and (510) for $H_2WO_4·H_2O$, respectively (JCPDS card no. 18-1420). The diffraction peaks (2θ at 16.6° and 26°) may be attributed to (110) and (002) of C. Therefore, the sample yielded diffraction peaks of $H_2WO_4·H_2O$ and C phases (curve a, Fig. 2), which indicated that the occurrence of the following chemical reaction: $Na_2WO_4+2HCl+H_2O→H_2WO_4·H_2O↓+2NaCl$. Crystal seed of H_2WO_4 can be formed homogenously in reaction suspension due to uniform dispersion of DWCNTs, Na_2WO_4 and HCl in EG (Fig. 3 left). In the absence of DWCNTs, the seeds will continue to expand along their own surface and will eventually coalesce to form larger particles that settle down and thereby affect the homogeneity of the mixture. The presence of dispersed nanotube bundles will prevent the union of the crystal seeds of H_2WO_4. Thereby the formation of secondary seed growth was restricted. This leads to the direct deposition and growth of H_2WO_4 seeds using DWCNT bundles as a support template (Fig. 3 right). Fig. 1a and the diffraction pattern of the C phase suggest DWCNTs are homogenously dispersed during the deposition of $H_2WO_4·H_2O$. Thus, H_2WO_4 sheet can be formed due to the bundle surface has not been covered completely by H_2WO_4 seeds. The morphology of the H_2WO_4 was also investigated by HRTEM. Several nanoparticles and nanotube bundles were observed (Fig. 1b). Sheet morphologies with length and width of 50 and 20 nm were observed when the morphology of the sample was magnified (Fig. 1c). In addition, CNTs were randomly found in the sample. The results indicated that the morphology of the deposited samples were correlated to that of DWCNTs. Sheet morphologies were formed when DWCNT bundles were partly surrounded by the deposited sample from the chemical reaction of Na_2WO_4 and HCl. Furthermore, nanosize sample was maintained if the resultant sheets were not in contact with each other. The visualizations were realized for dispersed DWCNT bundles that were homogenously distributed in the EG solvent. Therefore, DWCNT templates significantly influenced the size and morphology of the deposited sample from the reaction of Na_2WO_4 and HCl.

Thermoanalysis was performed to clarify the carbonization of the loaded as-prepared sample on DWCNTs. The TGA curve (curve 1, Fig. 1d) exhibited a reduced weight with increasing temperature. A sharp weight loss was observed in the sample when the temperature was increased from room temperature to 600 °C. This can be attributed to the decomposition of H_2WO_4 ($H_2WO_4→WO_3+H_2O$) from the reaction of Na_2WO_4 and HCl. The sample weights were slightly reduced for temperature reaching close to 1000 °C (Fig. 1d), which corresponded to the DTA curve (curve 2), with no obviously absorbable or exothermal peaks indicating that H_2WO_4 was completely decomposed at about 600 °C. Furthermore, it seems that reaction between the WO_3 and DWCNTs carbon source can not be occurred even temperature as high as 1000 °C.

The semifinished sample after heating to 600 °C and carbonization at 950 °C was further characterized using XRD based on thermoanalysis results. Clear characteristic peaks (Fig. 2b) with 2θ at 23.6°, 33.6°, 41.5°, 48.4° and 54.5° are found, which are indexed as (200), (220), (222), (400) and (420) planes of WO_3 (JCPDS card no. 46-1096). The results may be contributed to reaction of $H_2WO_4·H_2O→WO_3+2H_2O$. So, XRD patterns for the WO_3 phase (curve b) were observed. And DWCNTs can be burned completely with pumped air at 600 °C. The macro-morphologic feature of the sample is shown in ESI

Fig. S1b. ESI Fig. S2 reveals the morphology of the sample, SEM images and EDS results corresponded to the XRD data.

If the temperature was further increased to 950 °C, characteristic peaks (Fig. 2d) with 2θ at 31.6°, 35.7°, 48.5°, 58.5°,
5 64.3°, 73.5° and 77.2° are found, which are index as (001), (100), (101), (110), (111), (002) and (102) planes of WC (JCPDS card no. 65-4539). Therefore, the WC phase was clearly observed in the XRD pattern, and no W_2C phase existed in the sample. Another strong peaks at 40.3° would appeared if the temperature
10 was only increased to 850 °C (Fig. 2c, it is may be attributed to W_2C phase).The result indicats that liquid ethanol has undergone decomposition to form gaseous carbon source. The WO_3 phase was completely deoxidized to sufficiently contact with the gaseous carbon source from ethanol. Therefore, the WC phase
15 appeared after heating WO_3 at 950 °C in an N_2 environment. ESI Fig. S1c shows the macro-morphologic feature of WC. The carbonized temperature was low than traditional methods [14], the complete WC phase in the XRD pattern demonstrated that the microstructure of the tungstenic precursor of $H_2WO_4 \cdot H_2O$ and
20 liquid carbon sources significantly affected the formation of WC phase. EDS results from the selected area of SEM image (ESI Fig. S3) also implied that the atomic ratio of W and C was near 1:1. Gaseous carbon source can be obtained easily when liquid ethanol was heated. In addition, the gaseous carbon source can
25 easily move around to W atoms and deoxidized the tungstenic precursor. If DWCNTs were used as carbon souce (air was not pumped into reaction tube at 600 °C), WC can not formed due to high thermal stability of the DWCNTs which prevents the motion of carbon atoms around to W atoms at so low temperatures
30 (about 950 °C).

Figs. 4a and 4b illustrate the N_2 adsorption-desorption isotherms and the corresponding pore size distribution for H_2WO_4/DWCNTs before and after carbonization, respectively. The isotherms were obtained at 77 K, and the pore size
35 distributions were calculated from the desorption branch of N_2 isotherms via BJH method [35]. The specific surface areas of H_2WO_4/DWCNTs and WC from the BET method were found to be 39.8 and 16.2 m^2g^{-1}, respectively. The corresponding total pore volumes were 0.1023 and 0.0566 m^3g^{-1} ($P/P_0 = 0.966$),
40 suggesting that the sample exhibited higher specific surface areas and pore volumes compared to traditional products [14]. The results were attributed to the prepared nanosize $H_2WO_4 \cdot H_2O$ and WC with sheet morphologies. The reduced specific surface area and pore volume indicated a different morphology of WC when
45 $H_2WO_4 \cdot H_2O$ was heated and carbonized. The result was caused by porous structures that diffuse C atom into W, highly crystalline WC occupied certain pores.

Fig. 5 shows the TEM, EDS and HRTEM images of WC–Pt materials that are prepared in homogenous EG systems. Pt
50 particles were uniformly precipitated on the supports (Figs. 5a to 5d). Several nanosize materials conglomerated on each other, and nanosheets were also observed (Fig. 5b). Lengths and widths of the nanosheets varied from 60 nm to 500 nm, which were larger than those of nanoparticles. Most of the nanoparticles were
55 scattered on or around the nanosheets. Figs. 5c and 5d reveal the homogeneous distribution of the nanoparticles with sizes that range from 3 nm to 5 nm. The inter-planar distances (Fig. 5d) showed the nanoparticles are Pt particles. The EDS result (Fig. 5e,

selected area in Fig. 5b) indicated that the Pt loading is about 10
60 wt.%. In addition, the atomic ratio of W and C is about 1:1 also can be showed (this is also corresponding to Fig. 2d result). The Cu peak observed in the EDS spectrum arises from the Cu grid used for preparation of TEM sample. This observation suggests that the nanosheet is probably WC, and the composite is
65 composed of WC and Pt. The inter-planar distances measured in the HRTEM (Fig. 5e) image was about 0.23 nm, 0.2 nm, and 1.2 nm, which was in accordance with the (111), (200) and (311) facets of Pt (JCPDS card no. 04-0802, XRD data Fig. 6). It is implied that the small-size nanoparticles were Pt particles which
70 were decomposition products from the H_2PtCl_6 precursors. Figs. 5f and 5g depict the typical morphology of the nanosheets with a length and width of about 80 nm and 60 nm. Lattice fringes indicated the highly crystalline structure of the prepared WC with sheet morphologies. The inter-planar distances measured in the
75 HRTEM (Fig. 5g) image was about 0.29 nm, which was in accordance with the (001) facets of WC, the result was consistent with XRD data (Fig. 2).

WC–Pt respectively exhibited a current density and electrochemically active surface area of 0.011 A cm^{-2} and 66.67
80 m^2g^{-1} (Fig. 7), which indicated a highly electrochemical activity given that 10 wt% Pt was used in the study. Small-valued peaks were observed in CV curves (ESI Fig. S4) if the prepared WC nanosheet was used to measure electrochemical activity. Therefore, synergistic and catalytic properties of the WC
85 nanosheet in the catalyst could be speculated.

The high electrochemical activity of the nanosheets was attributed to the morphology and nanosize sheet characteristic of the prepared WC phase. Sheet morphology and nanosize features of the materials were affected by the DWCNT template, WO_3 and
90 WC could be prepared by carbonization. In addition, small sizes of WC that were prepared at low carbonization temperatures were maintained. Furthermore, the liquid carbon source was evaporated at carbonized temperature, and a sufficient contact between the gaseous carbon source and WO_3 was ensured.
95 Therefore, WC nanosheets could be prepared by in situ DWCNT templates and liquid carbon sources at low carbonization temperatures.

4. Conclusions

WC nanosheets were prepared with lengths and widths that
100 varied from 60 nm to 500 nm by using highly dispersive DWCNTs as the template. Addition of HCl into DWCNT and tungstenic precursor suspension formed H_2WO_4 seeds, in which the crystal seed was deposited on DWCNT bundles as supports. The second growth of the crystal grain of H_2WO_4 could be
105 restrained because of homogenous DWCNTs that were dispersed in EG solvent. Therefore, H_2WO_4 sheets could be prepared with length and width of about 50 and 20 nm, respectively. WC with a homogenous phase and good crystallization could be prepared after heating the prepared H_2WO_4 with a pumped liquid carbon
110 source. WC sheets could be potentially applied in electrochemistry, horniness alloys and other related fields because of their interesting morphologies and sizes.

RSC Advances Accepted Manuscript

Notes and references

[a] *Engineering Research Center of High-efficiency Development and Application Technology of Tungsten Resources (Ministry of Education), School of Materials Science and Engineering, Jiangxi University of Science and Technology, 86 Hong Qi Road, Ganzhou 341000, P. R. China. Fax: +86 797 8312422; Tel: +86 797 8312422; E-mail: wuziping724@mail.jxust.edu.cn*
[b] *Chemistry Department, College of Staten Island, City University of New York, 2800 Victory Boulevard, New York, 10314, United States*
[c] *Department of Mechanical, Aerospace and Nuclear Engineering, Rensselaer Polytechnic Institute, 110 8th St, Troy, 12180, United States*
† Electronic Supplementary Information (ESI) available: [details of any supplementary information available should be included here]. See DOI: 10.1039/b000000x/

1 A. Kumar, K. Singh and O. P. Pandey, Ceram. Int., 2011, **37**, 1415-1422.
2 K. Feng, J. Xiong, L. Sun, H. Fan and X. Zhou, J. Alloy. Compd., 2010, **504**, 277-283.
3 B. Huang, L. D. Chen and Q. Bais, Scripta Mater., 2006, **54**, 441-445.
4 Z. Yan, M. Cai and P. K. Shen, Science Reports, 2013, **3**, 1646-1-7.
5 G. R. Goren-Muginstein, S. Berger and A. Rosen, Nanostruct. Mater., 1993, **3**, 19-30.
6 J.P. C. Urbina, C. Daniel and C. Emmelmann, Physics Procedia, 2013, **41**, 752-758.
7 L. Bennett, J. R. Cuthill, A. Mcalister, N. Erickson and R. Watson, Science, 1975, **187**, 858-859.
8 K. M. Tsai, Int. J. Refract. Met. H. Mater., 2011, **29**, 188-201.
9 V. Keller, P. Wehrer, F. Garin, R. Ducros and G. Maire, J. Catal., 1995, **153**, 8-16.
10 C. D. Patrick, L. L. Jean and P. Claude, Catal, Today, 2001, **65**, 195-200.
11 P. Hasin, J. Phys. Chem. C, 2014, **118**, 4726–4732.
12 M. V. Iyer, L. P. Norcio, E. I. Kugler and D. B. Dadyburjor, Ind. Eng. Chem. Res., 2003, **42**, 2712-2721.
13 N. Ji, T. Zhang, M. Y. Zheng, A. Q. Wang, H. Wang, X. D. Wang and J. G. G Chen Angew. Chem. Int. ED., 2008, **47**, 8510-8513.
14 E. Antolini and E. R. Gonzalez, Appl. Catal. B: Enviro., 2010, **196**, 245-266.
15 C. A. Ma, C. B. Xu, M. Q. Shi, G. H. Song and X. L. Lang, J. Power Sources, 2013, **242**, 273-279.
16 H. Binder, A. Kohling, W. Kuhn, W. Lindner and G. Sandstede, Nature, 1969, **224**, 1299-1300.
17 D. Baresel, W. Gellert, J. Heidemeyer and P. Scharner, Angew. Chem. Int. Ed., 1971, **10**, 194-195.
18 Z. X. Yan G. Q. He, M. Cai, H. Meng and P. K. Shen, J. Power Sources, 2013, **242**, 817-823.
19 H. Chhina, S. Campbell and O. Kesler, J. Power Sources 2007, **164**, 431-440.
20 M. Rahsepar, M. Pakshir, P. Nikolaev, A. Safavi, K. Palanisamy and H. Kim, Appl. Catal. B: Enviro., 2012, **127**, 265-2729.
21 D.R. Mclntyre, G.T. Burstein and A. Vossen, J. Power Sources 2002, **107**, 67-73
22 J.B. Christian, S. P. E. Smith, M. S. Whittingham and H. D. Abruua, Electrochem. Commun. 2007, **9**, 2128-2132.
23 A. R. Ko, Y. W. Lee, J. S. Moon, S. B. Han, G. Z. Cao and K. W. Park, Appl. Catal. A: Gen., 2014, **477**, 102-108.
24 V.S. Palanker, R.A. Gajyev and D. Sokolsky, Electrochim. Acta 1977, **22**, 133-136
25 H. Okamoto, G. Kawamura, A. Ishikawa and T. Kudo, J. Electro. Soc. 1987, **134**, 1645-1658.
26 G. D. Rieck, Tungsten and its compounds, England: Pergamon Press, 1967.
27 C. Liang, F. Tian, Z. Wei, Q. Xin and C. Li, Nanotechnology, 2003, **14**, 955-958.
28 F. F. P. Medeiros, S. A. D. Oliveira, C. P. D. Souza, A. G. P. D. Silva, U. U. Gomes and J. F. D. Souza, Mater. Sci. Eng. A, 2001, **315**, 58-62.
29 C. H. Liang, L. Ding, C. Li, M. Pang, D. S. Su, W. Z. Li and Y. M. Wang, Energy Environ. Sci., 2010, **3**, 1121-1127.
30 C. L. Guo, Y. T. Qian and P. J. Han, J. Nanomater., 2011, 987530-1-5.
31 Z. P. Wu, J. N. Wang and J. Ma, Carbon, 2009, **47,** 324-327.
32 L.F. Su, J. N. Wang, F. Yu, Z. M. Sheng, H. Chang, and C. Pak, Chem. Phys. Lett. 2006, **420**, 421-425.
33 Z. P. Wu, M. M. Li, Y. Y. Hu, Y. S. Li, Z. X. Wang, Y. H. Yin, Y. S. Chen and X. Zhou, Scripta Mater., 2011, **64**, 809-812.
34 B. C. Lippens and J. H. De Boer, J. Catal. 1965, **4**, 319-413.
35 Z. Slanina and J. F. Crifo, Int. J. Thermophys., 1992, **13**, 465-476.

RSC Advances Accepted Manuscript

Graphical Abstract
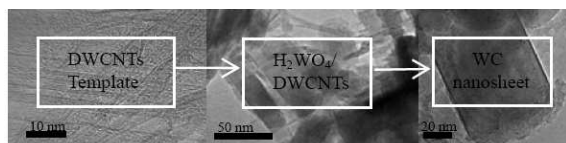
H$_2$WO$_4$ sheets about 50 nm long and 20 nm wide were prepared by DWCNTs

template, and WC nanosheets with high surface areas were obtained when the H$_2$WO$_4$

was carbonized at a low temperature using a liquid carbon source.
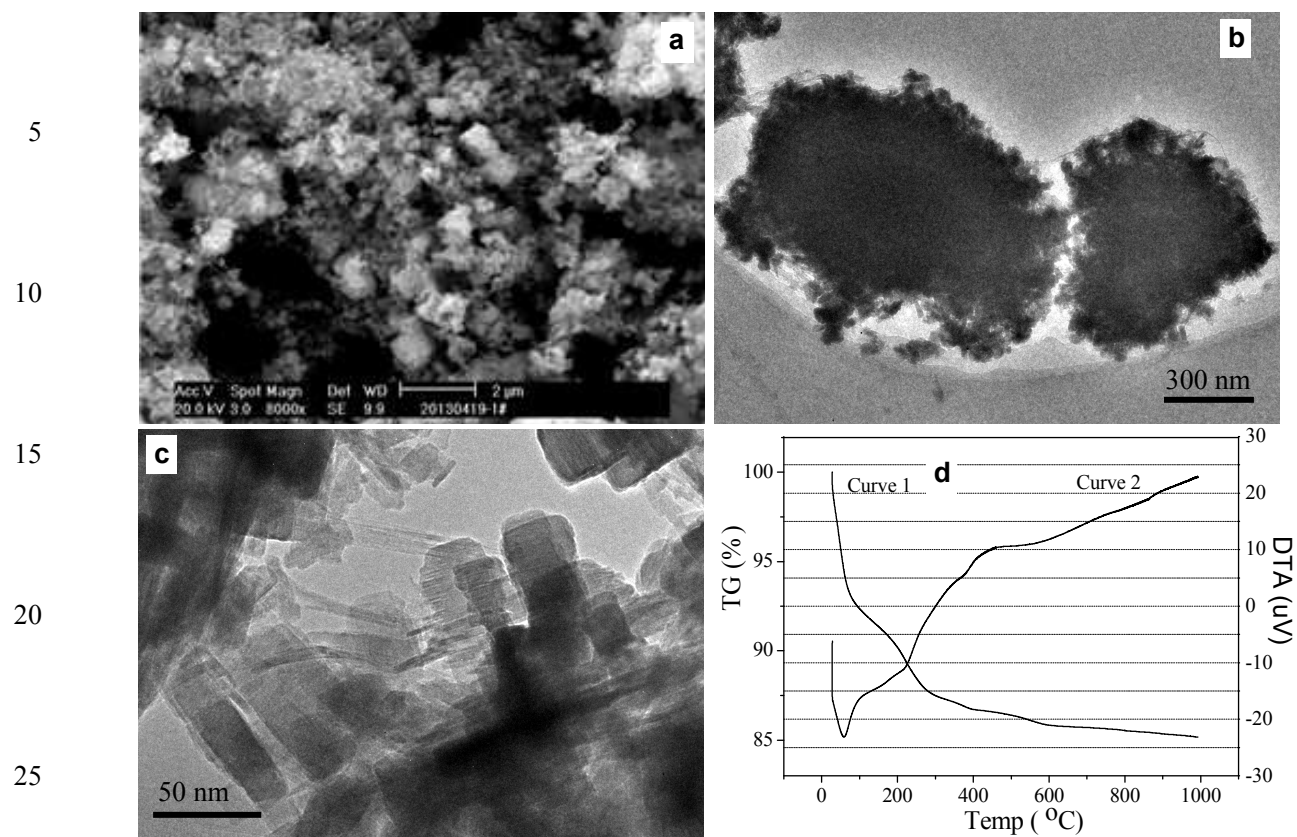
Fig. 1 Typical SEM image (a), HRTEM images (b, c) and TGA curves (d) of the semifinished sample

prepared from DWCNTs/EG suspension, Na_2WO_4 and HCl

7
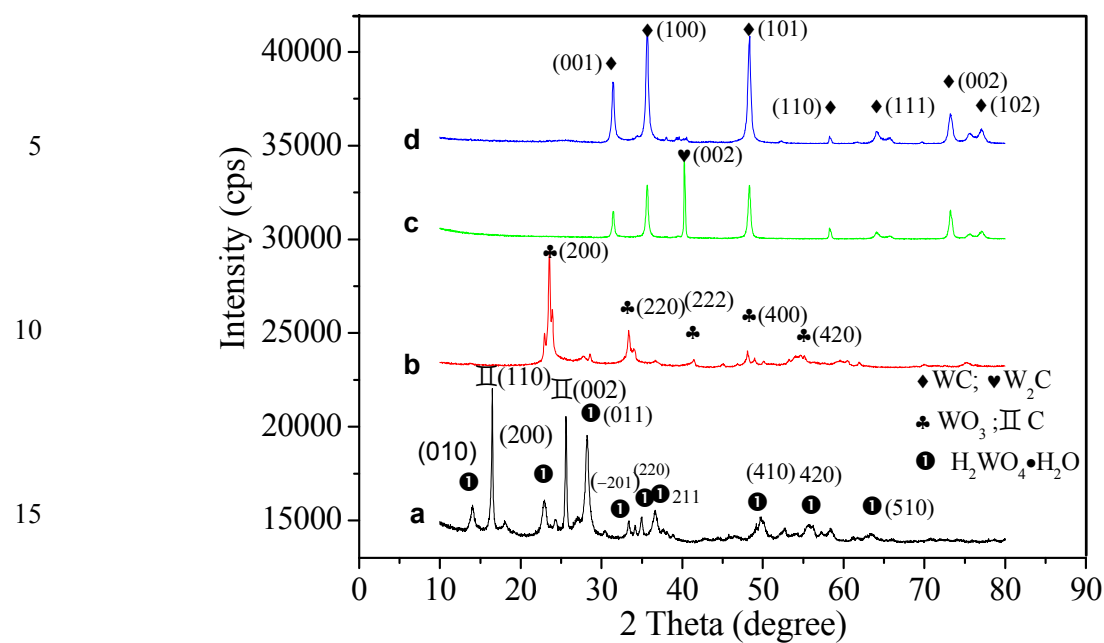
Fig. 2 XRD patterns of the semifinished sample before (a) and after (b) heated to 600 °C, and

carbonized at (c) 850 °C and (d) 950°C

8
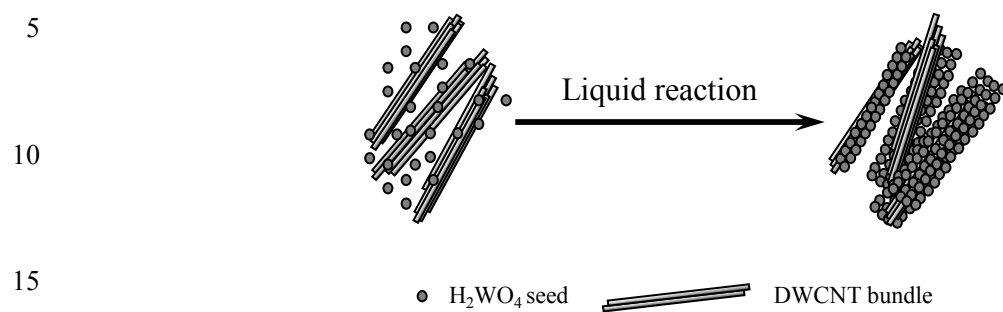
Fig.3 Schematic illustration of crystal seeds of H_2WO_4 deposited on DWCNT and formed nanosheet

9
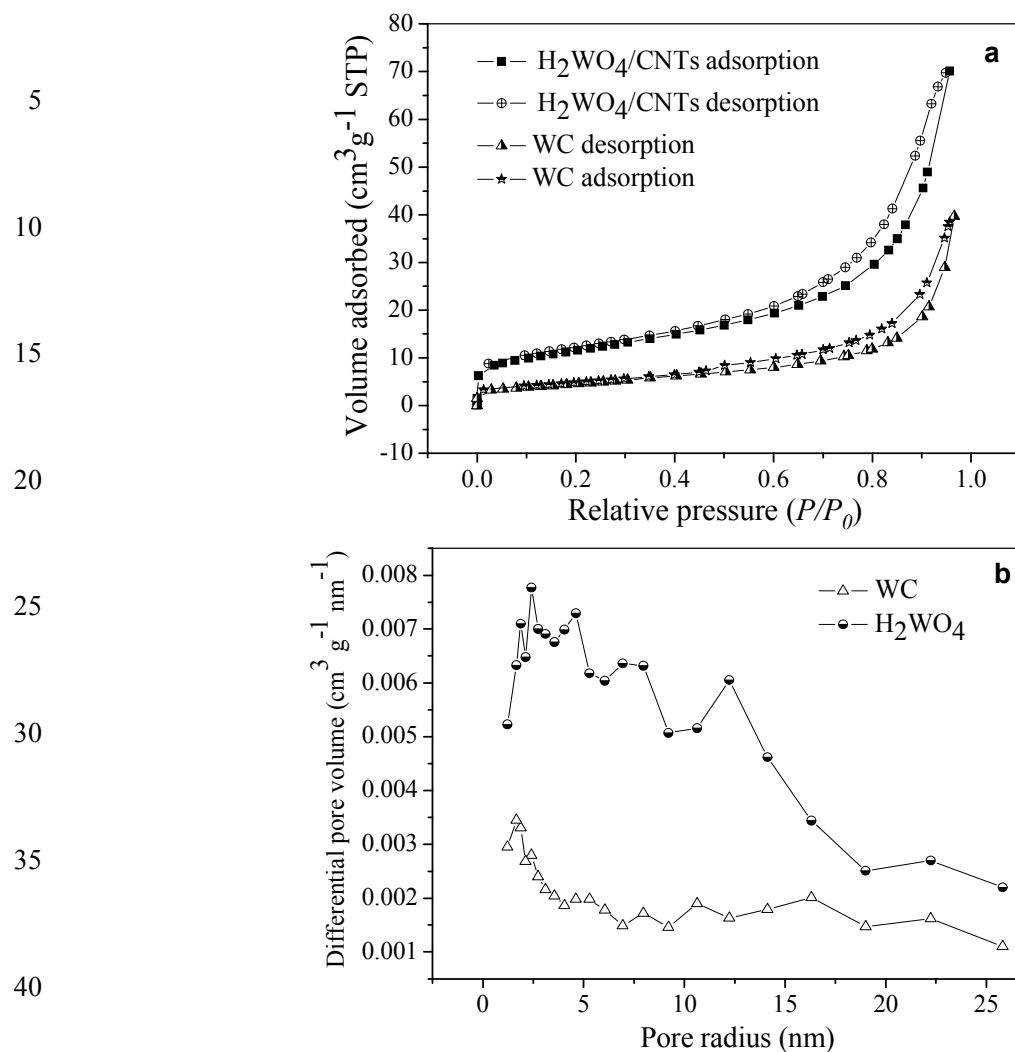
Fig. 4 N_2 adsorption/desorption isotherms (a) and pore radius distributions (b) of the semifinished

sample before and after heated to 600 °C, and carbonized at 950 °C
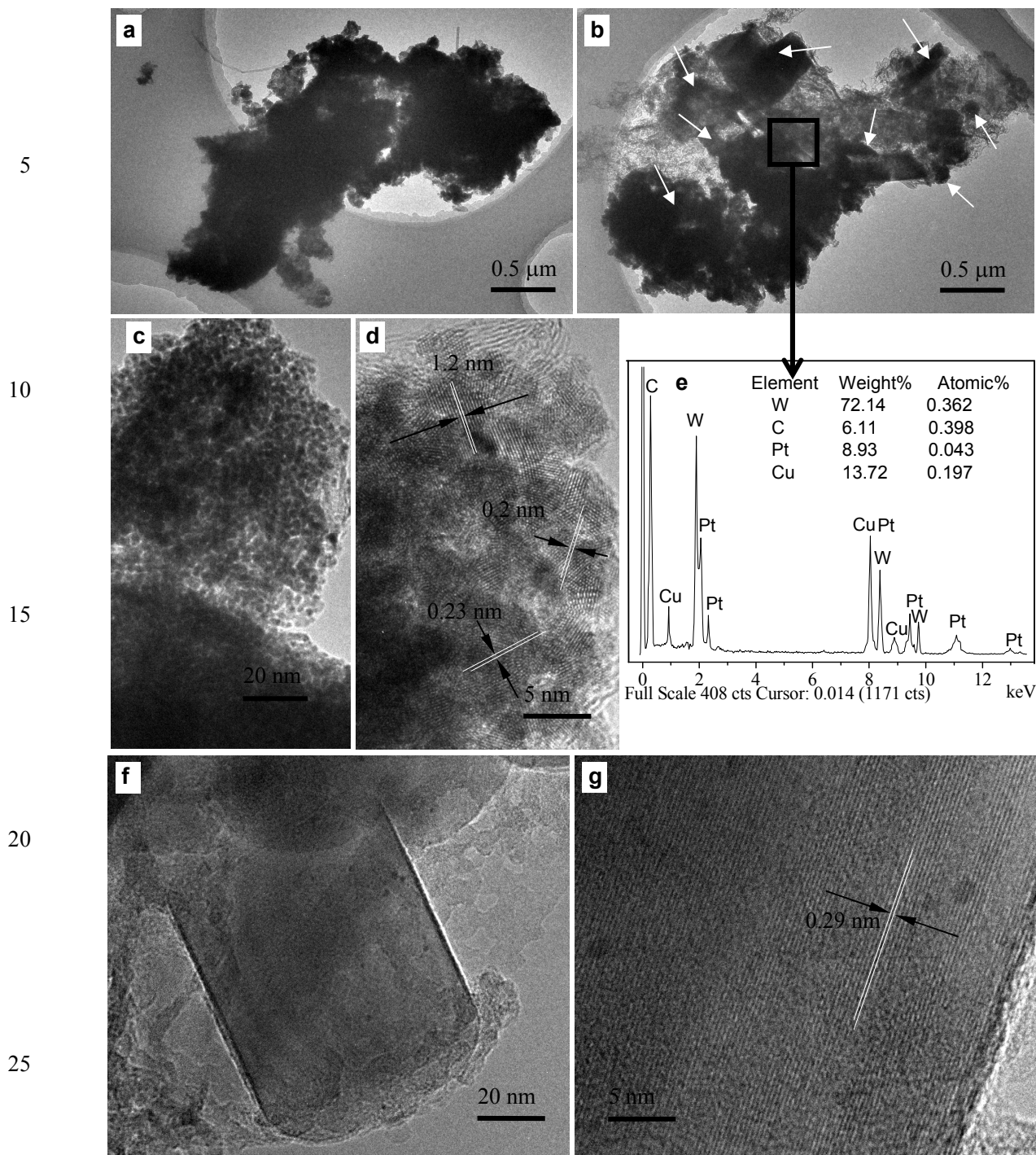
Fig. 5 Typical TEM, EDS and HRTEM images of WC-Pt material prepared in homogenous EG
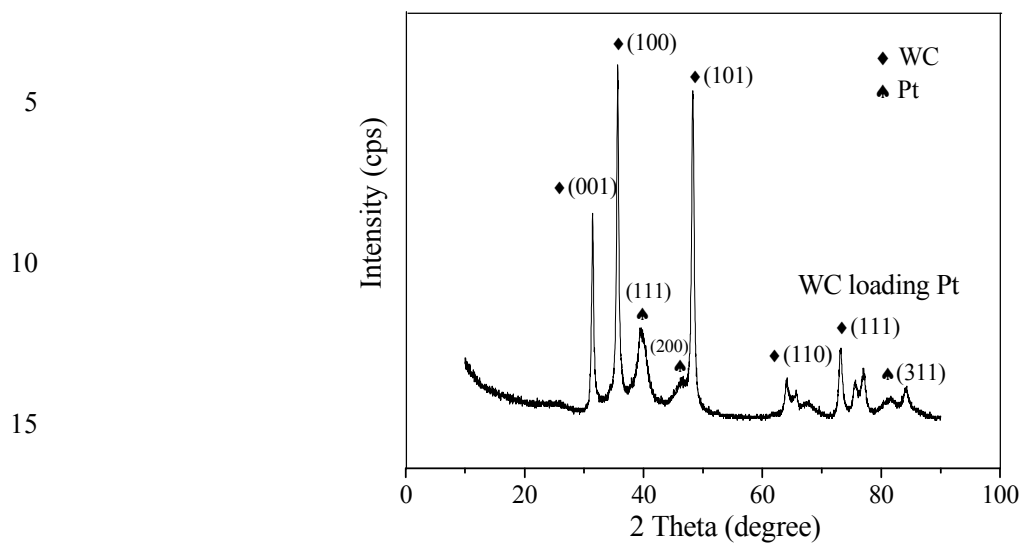
systems

Fig. 6 XRD pattern of WC-Pt material prepared in homogenous EG systems

12

5

10
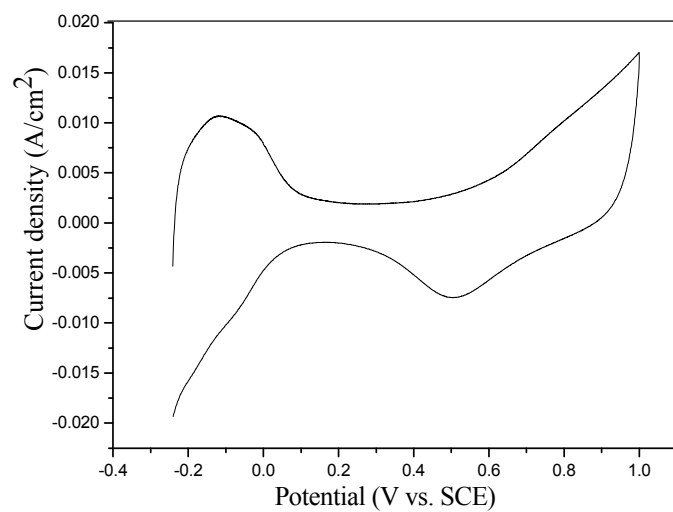
Fig. 7 CV curve of WC-Pt material at a scanning rate of 100 mv· s^{-1}. Note: WC-Pt material loading on

the working electrode was controlled to be 0.2 mg cm^{-2}

13